Supplementary material

Biomechanics and Modeling in Mechanobiology

Computational biomechanical assessment of stent-graft migration risk in different thoracic endovascular aortic repair (TEVAR) strategies for left subclavian artery reconstruction

Authors: Liu Yang[a,※], Kun Li[b,※], Meixuan Li[a], Jianming Li[a], Yunhan Cai[a], Qingsheng Lu[b,*], Shengzhang Wang[a,*]

[a] School of Biomedical Engineering, Fudan University, Shanghai, China

[b] Department of Vascular Surgery, Changhai Hospital, Naval Medical University, Shanghai, China

※ Co-first authors

* Corresponding authors

Email: Qingsheng Lu: luqs@newvascular.cn;

Shengzhang Wang: szwang@fudan.edu.cn.

Supplementary Fig. 1. Three-month follow-up CTA image after TEVAR.

Supplementary Table 1. Material properties of Castor stent-graft's Nitinol

Nitinol	**D=0.02inch**	**D=0.018inch**	**D=0.011inch**
Austenite elastic modulus E_A, MPa	28070	25800	20940
Austenite Poisson's ratio v_A	0.33	0.33	0.33
Martensite elastic modulus E_M, MPa	24650	25360	25640
Martensite Poisson's ratio v_M	0.33	0.33	0.33
Transformation strain ε^L	0.041	0.04	0.042
Start of transformation (loading) σ_L^s, MPa	395	429	444
End of transformation (loading)σ_L^E, MPa	497	494	453
Start of transformation (unloading)σ_U^s, MPa	70	117	104
End of transformation (unloading)σ_U^E, MPa	35	50	52
Start of transformation stress in compressσ_{CL}^S, MPa	592	643	666
Volumetric transformation strain ε_V^L	0.041	0.04	0.042
Densityρ,g/cm^3	6.5	6.5	6.5

Supplementary Table 2. Material properties of Talos and Fluency stent-graft's Nitinol

Nitinol	**Talos D=0.02inch**	**Talos D=0.018inch**	**Fluency**
Austenite elastic modulus E_A, MPa	25932	25127	20940
Austenite Poisson's ratio v_A	0.33	0.33	0.33
Martensite elastic modulus E_M, MPa	15248	14995	25640
Martensite Poisson's ratio v_M	0.33	0.33	0.33
Transformation strain ε^L	0.045	0.046	0.042
Start of transformation (loading) σ_L^s, MPa	572.1	556.5	444
End of transformation (loading)σ_L^E, MPa	637.5	619.4	453
Start of transformation (unloading)σ_U^s, MPa	327.9	299.5	104
End of transformation (unloading)σ_U^E, MPa	318.7	298.1	52
Start of transformation stress in compressσ_{CL}^S, MPa	572.1	556.5	666
Volumetric transformation strain ε_V^L	0.045	0.046	0.042
Densityρ,g/cm^3	6.5	6.5	6.5

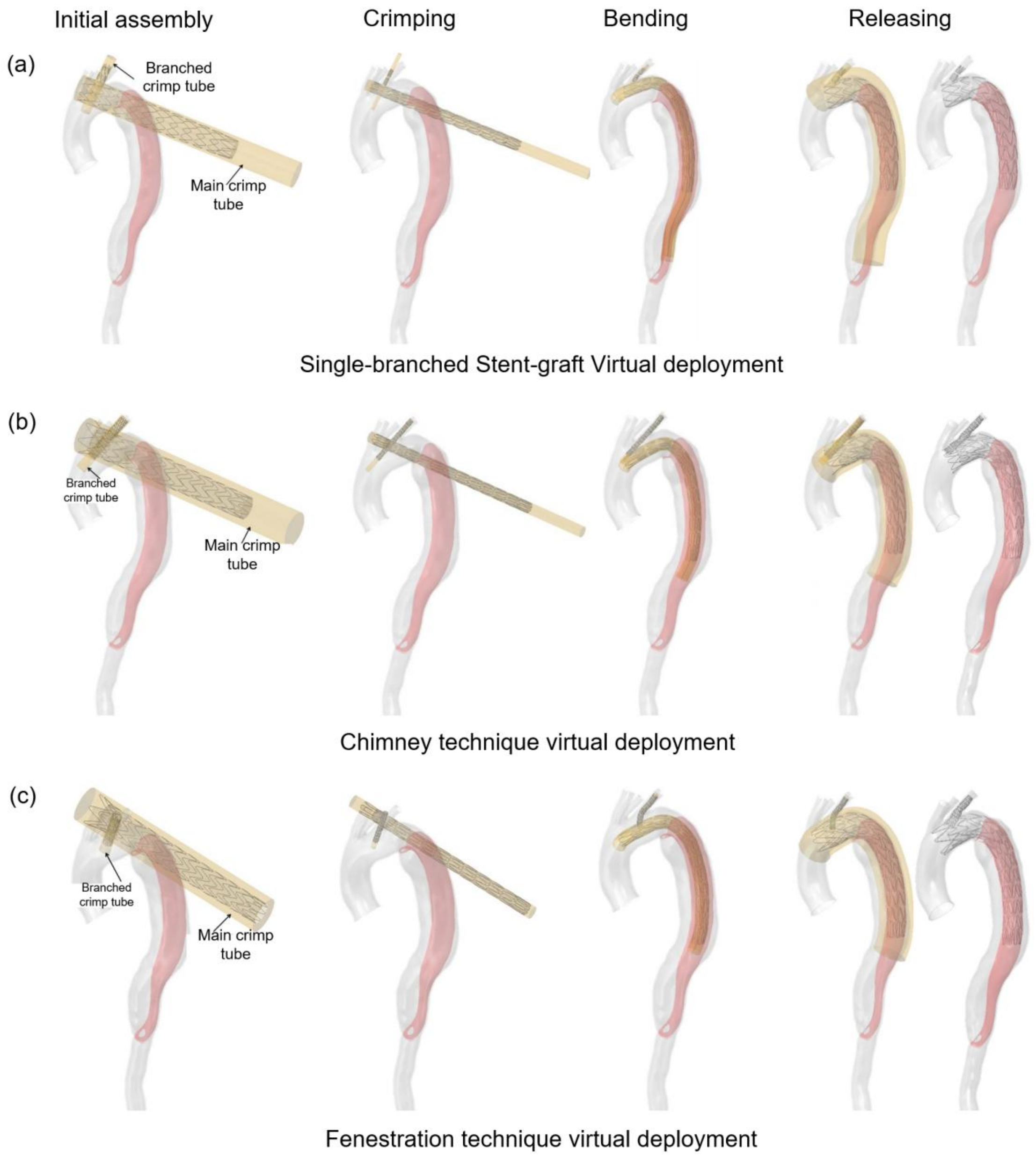

Supplementary Fig. 2. Detailed virtual deployment of three TEVAR strategies, including three procedures: crimping, bending and releasing; (a) Detail virtual deployment of single-branched SG; (b) Detail virtual deployment of chimney technique; (c) Detail virtual deployment of fenestration technique.

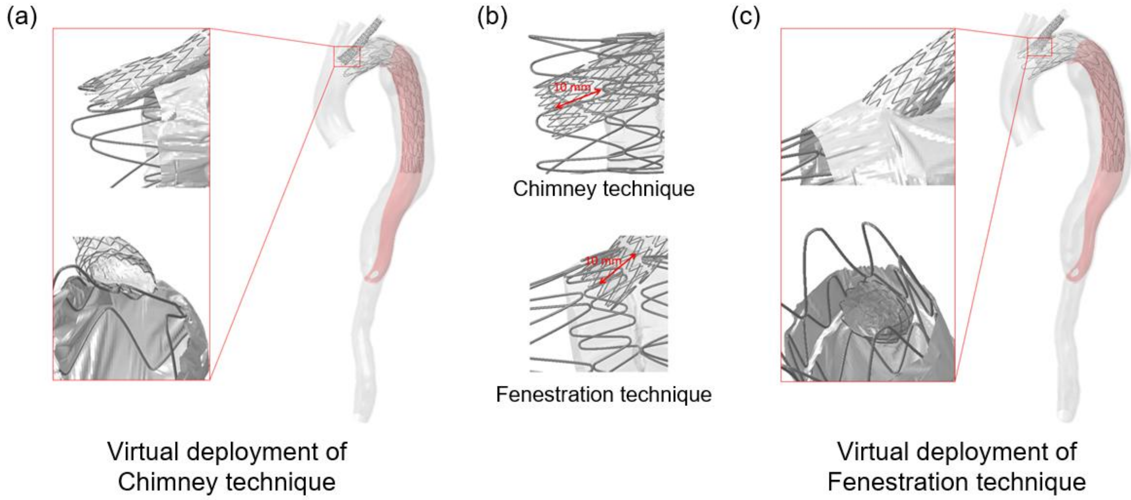

Supplementary Fig. 3. Virtual deployment results of chimney and fenestration techniques and their local magnification images; (a) Virtual deployment result of chimney technique and its local magnification images; (b) the branch SG in each technique extends 10 mm beyond the main-body SG; (c) Virtual deployment result of fenestration technique and its local magnification images.

Supplementary Table 3. Volume mesh sensitivity analysis of the fluid domain

Basic mesh size	4 mm	3.5 mm	3 mm	2.5 mm
Main-body SG DF (N)	12.38758157	12.37349073	12.3947316	12.39216872
Branch SG DF (N)	0.467399737	0.467001549	0.468111952	0.468301755

Supplementary Table 4. Boundary-layer mesh sensitivity analysis of the fluid domain

First prism-layer thickness	0.07 mm	0.06 mm	0.05 mm	0.04 mm
Main-body SG DF (N)	12.26522022	12.27240563	12.25316571	12.23552129
Branch SG DF (N)	0.467635929	0.467517885	0.466929565	0.465819852